Reactivity of cobalt(II)-dichalcogenide complexes: correlation between redox conversion and ligand-field strength

Marvelous, C.

Chapter 3

Cleaner and Stronger: How 8-quinolinolate Facilitates Formation of Co(III)-thiolate from Co(II)-disulfide Complexes

The formation of Co(III)-thiolate complexes from Co(II)-disulfide complexes using the anionic ligand 8-quinolinolate ($quin^-$) has been studied experimentally and quantum chemically. Two Co(II)-disulfide complexes $[Co_2(L^xSSL^x)(Cl)_4]$ (x=1 or 2; L^1SSL^1 = 2,2'-disulfanediylbis(N,N-bis(pyridin-2-ylmethyl)ethan-1-amine; L^2SSL^2 = 2,2'-disulfanedylbis(N-((6-methylpyridin-2-yl)methyl)-N-(pyridin-2-ylmethyl)-ethan-1-amine) have been successfully converted with high yield to their corresponding Co(III)-thiolate complexes upon addition of the ligand 8-quinolinolate. The unexpected formation of $[Co_2(L^2SSL^2)(quin)_2(Cl)_2]$ suggests a potential mechanism for the formation of the Co(III)-thiolate compound. Using density functional theory (DFT) computations the d-orbital splitting energies of the cobalt-thiolate compounds $[Co(L^1S)(quin)]^+$ and $[Co(L^2S)(quin)]^+$ were estimated to be 3.10 eV and 3.07 eV, confirming that the ligand-field strength of the ligand L^2SSL^2 is smaller than that of L^1SSL^1. Furthermore, the orientation of the $quin^-$ ligand in the thiolate compounds is imperative, as it determines the strength of the electrostatic interaction between $quin^-$ and the thiolate complex. The results suggest that coordination of the oxygen atom of the $quin^-$ ligand trans to the sulfur atom of the $[Co(L^1S)]^{2+}$ fragment benefits from more electrostatic attraction between aromatic rings.

This chapter will be published as a full article: Christian Marvelous, Lucas de Azevedo Santos, Maxime A. Siegler, Célia Fonseca Guerra, and Elisabeth Bouwman, *submitted*

3.1. Introduction

Electron transfer is part of many chemical and important biological processes, some examples including respiration and detoxification.[1-3] Transition-metal ions and sulfur-based ligands engage in such electron-transfer processes, as both species are susceptible to redox changes, leading to the formation and reduction of disulfide bonds of cysteines. One particular reaction that has been studied for two decades concerns the redox-conversion of transition-metal disulfide and thiolate complexes (**Scheme 3.1**).[4] In a typical reaction, two electrons from the two metal centers of a binuclear complex are transferred to the disulfide ligand. Consequently, the disulfide group is reduced into two thiolates, which then bind to the oxidized metal centers.

In recent years, the study of the redox-conversion reaction of disulfide and thiolate compounds has progressed from the copper-based system to other metal ions such as Mn, Fe, and Co.[5-9] The cobalt system in particular is interesting, as cobalt ions are involved in many enzymes and also because the redox-conversion of cobalt-based systems is relatively unexplored. Several reports describe the redox-conversion between cobalt(II)-disulfide and cobalt(III)-thiolate compounds induced chemically by addition or removal of halide ions, or by changing the solvent system.[6, 8, 10] Recently, we reported the redox-conversion of cobalt(II)-disulfide compounds to their corresponding cobalt(III)-thiolate compounds by the addition of the external ligand 2,2'-bipyridine (bpy).[11] It was hypothesized that the ligand-field strength of an added ligand would influence the formation of the cobalt(III)-thiolate complex, although bpy was found to be not suitable to induce this process.

In this Chapter we describe the results of our investigation on the effect of introducing 8-quinolinolate ($quin^-$) as the exogenous ligand to cobalt(II)-disulfide compounds of the ligands L^1SSL^1 (2,2'-disulfanediylbis(N,N-bis(pyridin-2-ylmethyl)ethan-1-amine) and L^2SSL^2 (2,2'-disulfanedylbis(N-((6-methylpyridin-2-yl)methyl)-N-(pyridin-2-ylmethyl) ethan-1-amine) (**Scheme 3.2**). In addition to the expected larger ligand-field strength, we

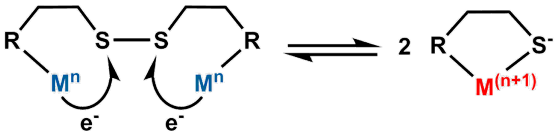

Scheme 3.1. Redox-conversion of metal-disulfide / metal-thiolate complex.

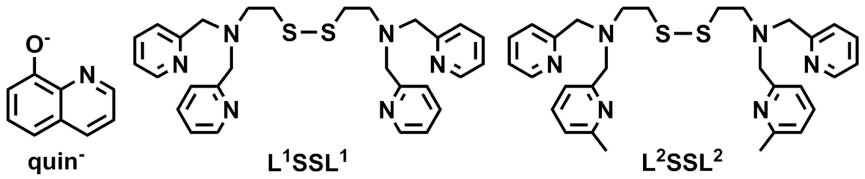

Scheme 3.2. Schematic representation of anionic ligand quin⁻ and the ligands L^1SSL^1 and L^2SSL^2 described in this Chapter.

hypothesized that the anionic quin⁻ ligand may compensate for the dicationic charge of the resultant thiolate compound and thus stabilize the relatively electron-poor Co(III) center. Furthermore, the larger aromatic conjugation and electron delocalization of quin⁻ in comparison with bpy might also contribute in some extent to the stabilization of a Co(III)-thiolate complex. Therefore, quin⁻ is expected to trigger a cleaner redox-conversion of cobalt(II)-disulfide compounds to the corresponding cobalt(III)-thiolate complexes than was found for bpy.

3.2. Results

3.2.1. Synthesis of the compounds

The ligands L^1SSL^1 and L^2SSL^2 were prepared according to published procedures with slight modifications and were obtained in good yields.[4, 9, 12] The synthesis and characterization of the disulfide compound $[Co_2(L^1SSL^1)(Cl)_4]$ ([**1**ss]) has been reported earlier.[8] The disulfide compound $[Co_2(L^2SSL^2)(Cl)_4]$ ([**2**ss]) was isolated as a purple powder in a yield of 72%. The ESI-MS spectrum of [**2**ss] in methanol (Figure AII.1) shows peaks at *m/z* 777.1 and 376.2 corresponding to the species $[\mathbf{2}ss - 2Cl^- + HCOO^-]^+$ and $[\mathbf{2}ss - 4Cl^- + 2HCOO^-]^{2+}$, respectively (formic acid was used in the eluting solvent, producing $HCOO^-$). The ^{1}H-NMR spectrum of compound [**2**ss] dissolved in CD_3CN (Figure AII.2) shows the presence of paramagnetic peaks from −16 ppm up to 44 ppm, confirming the presence of Co(II) centers. Further characterization using a magnetic susceptibility balance revealed the value of the magnetic moment to be 3.98 μ_B (calculated for each cobalt ion, spin-only magnetic moment 3.87 μ_B), in agreement with the presence of two high-spin Co(II) centers within the binuclear molecule. Finally, elemental analysis shows that the compound [**2**ss] was obtained analytically pure.

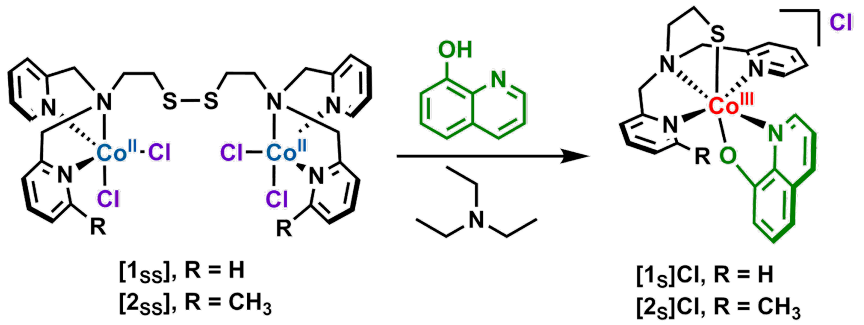

Scheme 3.3. Schematic representations of the cobalt compounds described in this work.

Addition of the ligand 8-quinolinol (Hquin) and triethylamine to solutions of *in-situ* generated [**1**$_{SS}$] or [**2**$_{SS}$] afforded the mononuclear cobalt(III)-thiolate compounds [Co(L^{1}S)(quin)]Cl ([**1**$_S$]Cl) and [Co(L^{2}S)(quin)]Cl ([**2**$_S$]Cl) (**Scheme 3.3**). Both [**1**$_S$]Cl and [**2**$_S$]Cl were obtained in nearly quantitative yield (96% and 99%, respectively) as brown powders. The ESI-MS spectrum of [**1**$_S$]Cl in methanol (Figure AII.3) shows a signal at *m/z* 461.1 corresponding to the cationic species [**1**$_S$]$^+$. Similarly, the ESI-MS spectrum of [**2**$_S$]Cl in acetonitrile (Figure AII.4) shows a signal at *m/z* 475.3 corresponding to [**2**$_S$]$^+$. The compounds [**1**$_S$]Cl and [**2**$_S$]Cl are diamagnetic both in the solid state as determined with a magnetic susceptibility balance as well as in solution as shown by the ^{1}H-NMR spectra (Figure AII.5−AII.10), in agreement with the presence of low-spin Co(III) ions. Both [**1**$_S$]Cl and [**2**$_S$]Cl can also be synthesized in the absence of triethylamine, although the ^{1}H-NMR spectra (Figures AII.11−AII.16) then show the presence of some impurities. Elemental analysis of both [**1**$_S$]Cl and [**2**$_S$]Cl shows that the compounds were obtained analytically pure after recrystallization. Single crystals of [**1**$_S$]Cl were grown using vapor diffusion of dry diethyl ether into a solution of [**1**$_S$]Cl in a 1:1 mixture of dry acetonitrile and dry methanol. Unexpectedly, after some time red single crystals were formed in the NMR tube containing the CD_3CN solution of [**2**$_S$]Cl, which turned out to be of the disulfide compound [Co$_2$(L^{2}SSL^2)(quin)$_2$(Cl)$_2$] ([**2**$_{SSquin}$]). Attempts to obtain single crystals of [**2**$_S$]Cl were not successful. However, dark brown single crystals of a compound containing [**2**$_S$]$^+$ were obtained after anion exchange reaction using vapor diffusion of dry diethyl ether into a dry acetonitrile solution containing [**2**$_S$]Cl and one equivalent of $AgSbF_6$. These single crystals

turned out to be of the silver-bridged, dinuclear compound $[[Co(L^2S)(quin)]_2Ag(MeCN)](SbF_6)_3$ ([**2s-Ag-2s**]$(SbF_6)_3$).

3.2.2. Description of the crystal structures

Crystallographic data of the structures are provided in Table AII.1. Compound [**1s**]Cl crystallizes in the triclinic space group *P*−1; the asymmetric unit contains one molecule of [**1s**]Cl and three co-crystallized molecules of methanol. Selected bond distances and angles are provided in **Table 3.1**. The cobalt center in [**1s**]Cl (**Figure 3.1.a**) is coordinated in an octahedral geometry by the sulfur donor and three nitrogen donor atoms of L^1S^-, as well as the oxygen and nitrogen donor atom of the $quin^-$ ligand. The octahedral geometry is slightly distorted, i.e. the largest deviation from perfect octahedral bond angles is 94.98° for S1−Co1−N31. These small deviations are caused by the 5-membered chelate rings formed

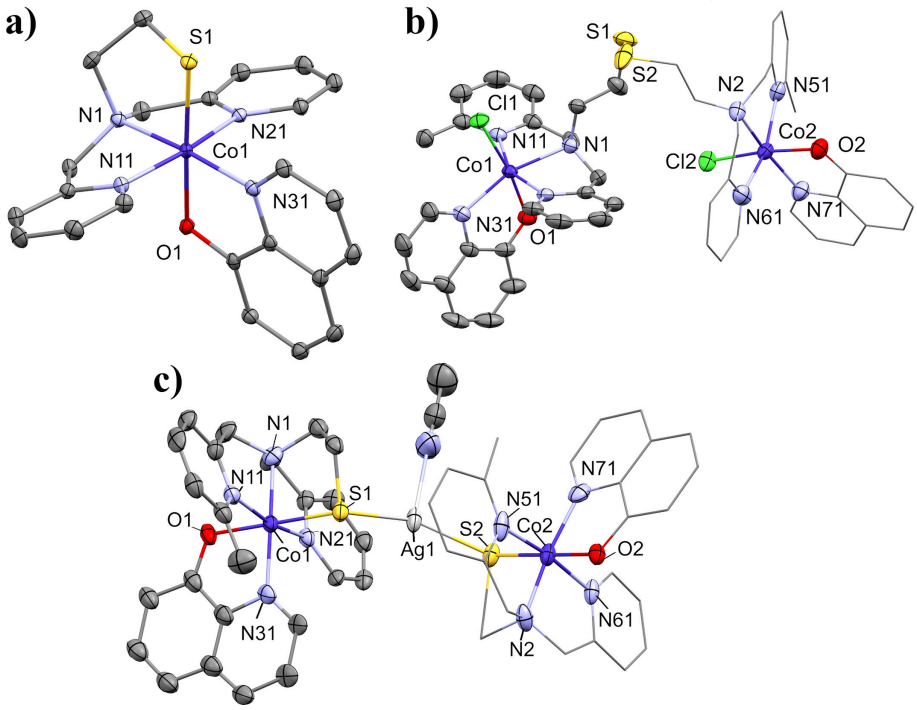

Figure 3.1. Displacement ellipsoid plots (50% probability) of a) [**1s**]$^+$, b) [**2**$_{SSquin}$], and c) [**2s-Ag-2s**]$^{3+}$ at 110(2) K. Parts of the binuclear molecule are displayed as wireframe for clarity. Hydrogen atoms, counter ions, disordered molecules, and lattice solvent molecules are omitted for clarity. The methyl groups in [**2**$_{SSquin}$] at sites of minor occupancy have been removed for clarity.

Table 3.1. Selected bond distances and bond angles in [**1S**]Cl.

Atoms	distance (Å)	Atoms	Bond angles (°)	Atoms	Bond angles (°)
Co1–N1	1.9523(13)	S1−Co1−N2	90.22(4)	O1−Co1−N31	85.29(6)
Co1–N11	1.9333(13)	S1−Co1−N11	93.91(4)	N1−Co1−N11	84.00(5)
Co1–N21	1.9231(13)	S1−Co1−N21	89.47(4)	N1−Co1−N21	85.98(5)
Co1–N31	1.9317(12)	S1−Co1−N31	94.98(4)	N1−Co1−N31	174.78(5)
Co1−O1	1.9638(11)	S1−Co1−O1	176.70(4)	N31−Co1−N11	95.24(5)
Co1–S1	2.2324(4)	O1−Co1−N2	89.53(5)	N31−Co1−N21	94.44(5)
Co1−Cl1	6.3536(5)	O1−Co1−N11	89.33(5)	N21−Co1−N11	169.43(6)
		O1−Co1−N21	87.24(5)		

by the ligand L^1S^- and $quin^-$. The three nitrogen atoms of L^1S^- are arranged in a meridional fashion, similar to the structure of $[Co(L^1S)(NCS)_2]$.[8] The oxygen atom of the $quin^-$ ligand is located *trans* to the thiolate donor atom, whereas the nitrogen donor of the $quin^-$ ligand is *trans* to the tertiary amine of L^1S. The Co−S bond distance is 2.232 Å, in agreement with other reports of low-spin cobalt(III)-thiolate compounds (2.19 – 2.30 Å, average bond distance = 2.252 Å).[8, 13, 14]

The distance between the non-coordinated chloride ion and the cobalt ion is 6.3536 Å. The chloride ion is in close proximity of three lattice methanol solvent molecules, tightly held by hydrogen bond interactions. The closest intermolecular distance between two thiolate sulfur atoms is 6.6478 Å. The distance between two cobalt centers in the unit cell is 9.8510 Å.

Compound [$\mathbf{2}_{\mathbf{SSquin}}$] crystallizes in the monoclinic space group $P2_1/n$. The structure of [$\mathbf{2}_{\mathbf{SSquin}}$] (**Figure 3.1.b**) is partly disordered, as the methyl groups in L^2SSL^2 are located partially on each of the two pyridine rings. The occupancy factors of the major positions of the disorder refine to 0.782(6) and 0.744(6). In the asymmetric unit, one dinuclear molecule and one molecule of acetonitrile are co-crystallized. Each cobalt(II) center is in a distorted octahedral geometry, bound to three nitrogen atoms of the ligand L^2S, the oxygen and nitrogen donor of one 8-quinolinolate ligand, and one chloride ion. The structure of this dinuclear compound resembles that of $[Co_2(L^1SSL^1)(bpy)_2(Cl)_2](BPh_4)_2$ reported in our previous study,[11] but in contrast to $[Co_2(L^1SSL^1)(bpy)_2(Cl)_2](BPh_4)_2$, the nitrogen donors of L^2SSL^2 are arranged in a meridional fashion, similar to the conformation in [**1S**]Cl. The chloride ion is coordinated *trans* to the oxygen donor of the $quin^-$ ligand, and the $quin^-$ nitrogen atom is *trans* to the tertiary amine of L^2SSL^2.

Selected bond distances and angles are listed in **Table 3.2**. The bond distances and bond angles related to the Co2 center are very similar to those of Co1. The S−S bond distance in [$\mathbf{2}_{\mathbf{SSquin}}$] is 2.022 Å, comparable to that in $[Co_2(L^1SSL^1)(bpy)_2(Cl)_2](BPh_4)_2$ (2.029) Å. The Co−Cl bond distance (2.412 Å) is longer than that in $[Co_2(L^1SSL^1)(bpy)_2(Cl)_2](BPh_4)_2$ (2.38 Å) or the disulfide compound [$\mathbf{1}_{\mathbf{SS}}$] (2.32 and 2.27 Å), indicating that the Co−Cl bond is relatively weaker, possibly due to a *trans* effect of the quin$^-$ oxygen donor. The Co–N (tertiary amine nitrogen) bond distances are unusually long (2.200 and 2.199 Å) compared to those in other compounds with similar coordination spheres (octahedral Co(II) with four nitrogen donor atoms, one oxygen donor atom and one chloride ion), which are on average 1.952 Å.[15, 16] The distances between the cobalt centers and the nearest disulfide sulfur atom are around 5.8 Å, which is slightly shorter than in [$\mathbf{1}_{\mathbf{SS}}$] (5.96 and 5.93 Å). The structure does not contain hydrogen bonds, but a short intermolecular contact of 3.340 Å between the methylated pyridine ring and the neighboring non-methylated pyridine ring indicates the presence of π-π stacking interactions. These π-π stacking interactions are in the parallel displaced conformation, most likely due to the different substituents (−CH_3 vs −H) in the interacting moieties.[17]

A displacement ellipsoid plot (50% probability) for [$\mathbf{2}_{\mathbf{S}}$**-Ag-**$\mathbf{2}_{\mathbf{S}}$]$(SbF_6)_3$ is depicted in **Figure 3.1.c** (as the 3+ cation). Bond distances and bond angles are provided in **Table 3.3**. The bond distances and bond angles around the Co2 center are similar to those of Co1. Compound [$\mathbf{2}_{\mathbf{S}}$**-μ-Ag-**$\mathbf{2}_{\mathbf{S}}$]$(SbF_6)_3$ crystallizes in the monoclinic space group $P2_1/c$. In the asymmetric unit, one cationic molecule [$\mathbf{2}_{\mathbf{S}}$**-Ag-**$\mathbf{2}_{\mathbf{S}}$]$^{3+}$ is co-crystallized with three SbF_6^- counter ions and one lattice acetonitrile solvent molecule. The cationic fragment [$\mathbf{2}_{\mathbf{S}}$**-Ag-**$\mathbf{2}_{\mathbf{S}}$]$^{3+}$ is composed of two [$\mathbf{2}_{\mathbf{S}}$]$^+$ complexes bridged by a silver ion to which one acetonitrile

Table 3.2. Selected bond distances and angles in [$\mathbf{2}_{\mathbf{SSquin}}$].

Atoms	distance (Å)	Atoms	Bond angles (°)	Atoms	Bond angles (°)
Co1–N1	2.200(2)	O1−Co1−Cl1	171.43(6)	Cl1−Co1−N31	93.92(7)
Co1–N11	2.192(2)	O1−Co1−N1	85.64(8)	N1−Co1−N11	78.45(8)
Co1–N21	2.179(2)	O1−Co1−N11	87.30(8)	N1−Co1−N21	77.49(9)
Co1–N31	2.132(2)	O1−Co1−N21	93.15(8)	N1−Co1−N31	161.88(9)
Co1–O1	2.0610(19)	O1−Co1−N31	78.97(8)	N31−Co1−N11	110.02(9)
Co1−Cl1	2.3921(7)	Cl1−Co1−N1	102.14(6)	N31−Co1−N21	93.75(9)
S1−S2	2.0223(19)	Cl1−Co1−N11	90.70(6)	N21−Co1−N11	155.83(9)
Co1−S1	5.848(1)	Cl1−Co1−N21	92.09(6)		

Table 3.3. Bond distances and bond angles in [**2s-Ag-2s**]$(SbF_6)_3$.

Atoms	distance (Å)	Atoms	Bond angles (°)	Atoms	Bond angles (°)
Co1–S1	2.2500(19)	S1−Co1−O1	176.4(4)	N1–Co1–N11	84.5(2)
Co1–O1	1.919(7)	S1−Co1−N1	90.23(18)	N1–Co1–N21	83.4(2)
Co1–N1	1.943(6)	S1−Co1−N11	88.73(17)	N1–Co1–N31	170.6(4)
Co1–N11	2.020(5)	S1−Co1−N21	92.49(17)	N31–Co1–N11	103.1(3)
Co1–N21	1.953(5)	S1−Co1−N31	95.4(4)	N31–Co1–N21	88.8(3)
Co1–N31	1.934(7)	O1– Co1–N1	91.1(4)	N21–Co1–N11	167.9(2)
S1−Ag1	2.452(3)	O1– Co1–N11	88.1(5)	S1–Ag1–S2	157.5(2)
S2−Ag1	2.4300(18)	O1– Co1–N21	91.0(5)	S1–Ag1–N91	112.7(2)
Ag1−N91	2.527(10)	O1– Co1–N31	83.7(5)	S2–Ag1–N91	89.3(2)

molecule is coordinated. The cobalt centers in the two [**2s**]$^+$ fragments are in slightly distorted octahedral geometries similar to [**1s**]$^+$, coordinated by one oxygen, one sulfur, and four nitrogen atoms. The Co−S bond distances are 2.2500(19) and 2.2612(19) Å, in agreement with the low-spin Co(III)-thiolate compound. The Ag^+ ion is in a T-shaped geometry; the S−Ag bond distances are 2.452(3) and 2.4300(28) Å, the S1−Ag−S2 bond angle is 157.5(2)°. The S−Ag bond distances in [**2s-μ-Ag-2s**]$(SbF_6)_3$ are typical, as compared to other structures with similar geometries having an average S−Ag bond distance of 2.413 Å.[18-21]

3.2.3. Solution studies of Co(II)-disulfide and Co(III)-thiolate compounds

Addition of 8-quinolinol together with triethylamine into solutions of the disulfide compounds [**1ss**] or [**2ss**] results in an immediate color change from purple to dark brown. The UV−visible spectrum of [**1ss**] in acetonitrile (**Figure 3.2.a**, solid blue line) is in accordance with the literature,[8] and matches the simulated spectrum (details are provided in the Experimental Section) (**Figure 3.2.a**, dashed blue line). The spectrum of [**2ss**] (**Figure 3.2.b**, solid blue line) is red-shifted compared to that of [**1ss**]. The two peaks in the spectrum of [**2ss**] are located at 545 nm (1.5×10^3 M^{-1} cm^{-1}) and 652 nm (8.5×10^2 M^{-1} cm^{-1}), and are ascribed to Co(II) *d-d* transitions reflecting a trigonal-bipyramidal geometry.[22, 23] Another Co(II) *d−d* transition is also visible at around 850−900 nm ($\varepsilon < 100$ M^{-1} cm^{-1}). The simulated spectrum of [**2ss**] (**Figure 3.2.b**, dashed blue line) has a reasonable match with the experimental spectrum, as the main features of the experimental spectrum are present.

The UV−visible spectra of dark brown solutions of [**1s**]Cl (**Figure 3.2.a**, black line) and [**2s**]Cl (**Figure 3.2.b**, black line) show peaks at 412 nm ($\varepsilon = 2.1 \times 10^4$ M^{-1} cm^{-1}) and 424 nm

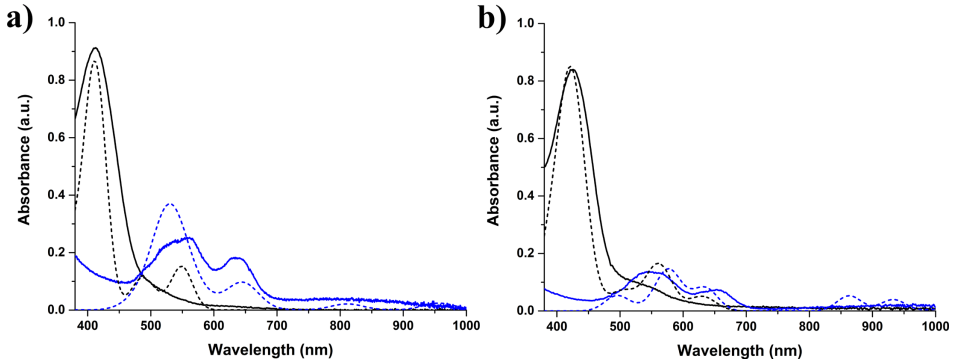

Figure 3.2. UV-visible spectra of **a)** 2 mM solution of [**1**$_{SS}$] (solid blue line) and 1 mM solution of [**1**$_{S}$]Cl (solid black line) in acetonitrile and **b)** 2.5 mM solution of [**2**$_{SS}$] (solid blue line) and 1 mM solution of [**2**$_{S}$]Cl (solid black line) in acetonitrile. Simulated spectra of the respective compounds are provided as dashed lines; the wavelength of the simulated spectra has been adjusted for clarity. UV-visible spectra were recorded using a transmission dip probe with path length of 0.14 mm. Simulated spectra were generated using TDDFT calculations.

($\varepsilon = 2.0 \times 10^4$ M^{-1} cm^{-1}), respectively, ascribed to a ligand-to-metal charge transfer transition (LMCT), most likely originating from the thiolate sulfur or quin$^-$ nitrogen donor.[14, 24] The simulated spectra of [**1**$_{S}$]Cl (**Figure 3.2.a**, dashed black line) and [**2**$_{S}$]Cl (**Figure 3.2.b,** dashed black line) confirm that both absorptions indeed originate from LMCT transitions.

3.2.4. Computational studies

In Chapter 2, we discussed the role of the ligand-field strength of the additional ligand in the redox conversion of the Co(II)-disulfide complex with the LSSL ligand scaffold.[11] In order to further validate the previous findings, we investigated the ligand-field strength of quin$^-$ using DFT to estimate the *d*-orbital splitting energies of the Co(III)-thiolate complexes. The structures of the cationic compounds [**1**$_{S}$]$^+$ and [**2**$_{S}$]$^+$ were optimized in low-spin singlet states (S=0). In addition, we were interested to investigate the influence of ligand orientation on the stability of the cobalt(III)-thiolate complex, as the conformation of the LS ligand scaffold has been shown to affect how the sulfur atom approaches the cobalt center. Therefore, geometry optimizations were also done for both cationic compounds in which the orientation of quin$^-$ is reversed, so that the nitrogen donor atom is *trans* to the thiolate sulfur, and the oxygen atom trans to the tertiary amine nitrogen ([**1**$_{S,rev}$]$^+$ and [**2**$_{S,rev}$]$^+$). The equilibrium geometries in the gas phase for [**1**$_{S}$]$^+$ and [**1**$_{S,rev}$]$^+$ with selected bond distances are depicted in **Figure 3.3**. Equilibrium geometries for [**2**$_{S}$]$^+$ and [**2**$_{S,rev}$]$^+$ in the gas phase are provided in Figure AII.17.

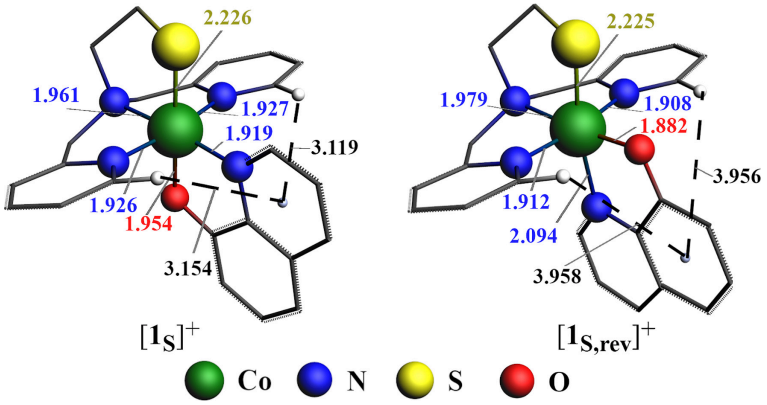

Figure 3.3. Equilibrium geometries of $[\mathbf{1}_S]^+$ and $[\mathbf{1}_{S,rev}]^+$ in gas phase with selected bond distances (in Å). Hydrogen atoms are omitted for clarity, except for hydrogen atoms of $[Co(L1S)]^{2+}$ facing $quin^-$ ligand. The closest distances between the *ortho*-hydrogen atoms of the pyridine groups and the center of the nearest $quin^-$ ring are depicted as dashed lines.

The cationic compounds $[\mathbf{1}_S]^+$ and $[\mathbf{2}_S]^+$ in methanol are about 5 to 6 kcal/mol more stable than $[\mathbf{1}_{S,rev}]^+$ and $[\mathbf{2}_{S,rev}]^+$, in agreement with the experimental results. The same trend in stability is observed in gas phase. That is, without solvent $[\mathbf{1}_S]^+$ and $[\mathbf{2}_S]^+$ are about 7 to 9 kcal/mol more stable than $[\mathbf{1}_{S,rev}]^+$ and $[\mathbf{2}_{S,rev}]^+$. Thus, the preference in orientation of $quin^-$ is not determined by the media. The gas phase equilibrium geometries of $[\mathbf{1}_S]^+$ and $[\mathbf{2}_S]^+$ are in good agreement with the geometries found in the crystal structures. The Co–S bond distances in the optimized structures of $[\mathbf{1}_S]^+$ or $[\mathbf{2}_S]^+$ are 2.225–2.226 Å, and the Co–O and Co–N bond distances are all within error range of those found in the crystal structures.

Attempts were undertaken to estimate *d*-orbital splitting energies of both $[\mathbf{1}_S]^+$ and $[\mathbf{2}_S]^+$ using the DFT method described in Chapter 2.[11] Similar to the results described in Chapter 2, for both $[\mathbf{1}_S]^+$ and $[\mathbf{2}_S]^+$, five non-degenerate molecular orbitals were found with large Co *d*-orbital contributions (Figures AII.18 and AII.19). These five non-degenerate molecular orbitals are distributed in two sets of energy levels roughly corresponding to the expected t_{2g} and e_g levels for octahedral ligand-field splitting. The energy difference between the highest and the lowest of these MO levels of $[\mathbf{1}_S]^+$ and $[\mathbf{2}_S]^+$ are slightly larger (by 0.2 eV) than that of $[Co(L^1S)(bpy)]^{2+}{}_{mer}$, indicative of a larger ligand-field strength of $quin^-$ compared to bpy. The energy difference of $[\mathbf{2}_S]^+$'s MO sets in a quantitative level is 3.07 eV, which is only slightly smaller than that of $[\mathbf{1}_S]^+$ (3.10 eV), indicating weaker ligand-field strength of the

ligand L^2SSL^2 compared to that of L^1SSL^1. However, care should be taken with such quantitative comparisons, as the five orbitals in the MO sets comprises not only large contributions of the Co *d*-orbitals, but also of the donor atoms of the ligands.

In order to explain the stability of $[\mathbf{1_S}]^+$ compared to $[\mathbf{1_{S,rev}}]^+$, and analogously of $[\mathbf{2_S}]^+$ compared to $[\mathbf{2_{S,rev}}]^+$, we investigated the $[Co(L^1S)]^{2+}$•••$[quin]^-$ bond formation using activation-strain analysis (see section 3.5.3 for details).[25, 26] We observed that ΔE_{strain} (that is the energy to deform) of both $[\mathbf{1_S}]^+$ and $[\mathbf{1_{S,rev}}]^+$ are very similar (with 0.8 kcal/mol difference), and therefore does not cause the stabilization of $[\mathbf{1_S}]^+$ over $[\mathbf{1_{S,rev}}]^+$ (see **Table 3.4**). Instead, the interaction energy ΔE_{int} of $[\mathbf{1_S}]^+$ is more stabilizing by 8.2 kcal/mol than that of $[\mathbf{1_{S,rev}}]^+$. Thus, the interaction between the two fragments $[Co(L^1S)]^{2+}$ and $[quin]^-$ defines the stabilization of $[\mathbf{1_S}]^+$ over $[\mathbf{1_{S,rev}}]^+$.

Next, we decomposed ΔE_{int} into Pauli repulsion energy (ΔE_{Pauli}), electrostatic interaction energy (ΔV_{elstat}), and orbital interaction energy (ΔE_{oi}), using energy-decomposition analysis (see section 3.5.3).[26, 27] The molecular-orbital diagram for the bonding interaction between $[Co(L^1S)]^{2+}$ and $[quin]^-$ is provided in Figures AII.20−AII.21. It is apparent from **Table 3.4** that the electrostatic interaction ΔV_{elstat} plays the most important role in stabilizing $[\mathbf{1_S}]^+$ over $[\mathbf{1_{S,rev}}]^+$, as ΔV_{elstat} is about 21 kcal/mol lower for $[\mathbf{1_S}]^+$ than for $[\mathbf{1_{S,rev}}]^+$.

The molecular electrostatic potential of both $[Co(L^1S)]^{2+}$ and $[quin]^-$ fragments in $[\mathbf{1_S}]^+$ and $[\mathbf{1_{S,rev}}]^+$ are shown in **Figure 3.4**. It was found that in both $[\mathbf{1_S}]^+$ and $[\mathbf{1_{S,rev}}]^+$ the positive charges are evenly spread out over the $[Co(L^1S)]^{2+}$ fragment. In $[quin]^-$ both the nitrogen and the oxygen atom are more negatively charged but the negative charge is delocalized over the carbon atoms of the aromatic rings. Therefore, the attraction between $[Co(L^1S)]^{2+}$ and $[quin]^-$ fragments is not only determined by the electrostatic interaction between the neighboring

Table 3.4. Energy terms derived from energy-decomposition analysis of $[\mathbf{1_S}]^+$ and $[\mathbf{1_{S,rev}}]^+$.

	Energy (kcal/mol)	
	$[\mathbf{1_S}]^+$	$[\mathbf{1_{S,rev}}]^+$
$\Delta E_{bond,methanol}$	−61.7	−55.7
ΔE_{bond}	−238.5	−229.6
ΔE_{strain}	12.4	13.2
ΔE_{int}	−251.0	−242.8
ΔV_{elstat}	−290.2	−269.1
ΔE_{Pauli}	183.6	159.8
ΔE_{oi}	−144.4	−133.4

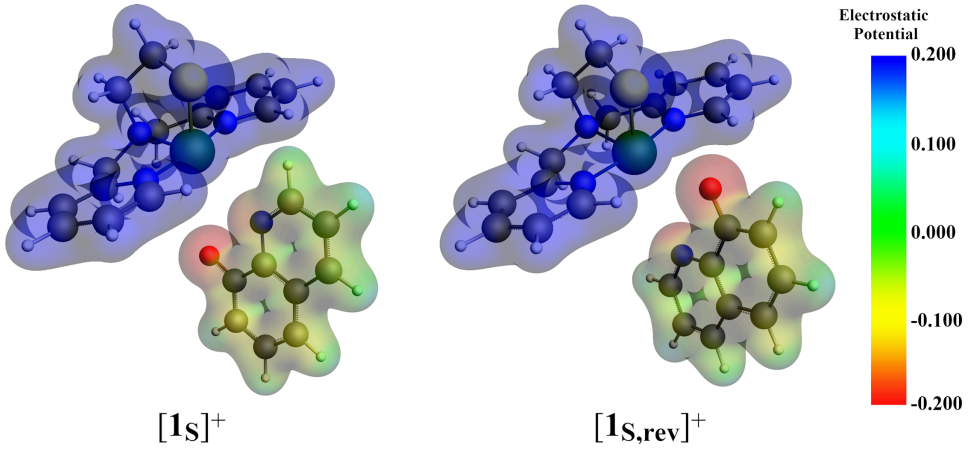

Figure 3.4. Electrostatic potential of $[Co(L^1S)]^{2+}$ and $[quin]^-$ fragments in $[\mathbf{1}_S]^+$ and $[\mathbf{1}_{S,rev}]^+$.

atoms but has a significant contribution from long-range interactions between the $[Co(L^1S)]^{2+}$ and $[quin]^-$ fragments. This is demonstrated by the distances of the *ortho*-hydrogen atoms of the pyridine rings to the aromatic ring in the $quin^-$ ligand (**Figure 3.3**) which are shorter in $[\mathbf{1}_S]^+$ (3.154 Å and 3.119 Å) than in $[\mathbf{1}_{S,rev}]^+$ (3.958 Å and 3.956 Å).

3.3. Discussion

We try to gain understanding of the influence of the ligand-field strength of the additional ligands on the redox-conversion of cobalt(II) disulfide compounds based on our LSSL scaffold. In Chapter 2 we described our study using the external ligand 2,2'-bipyridine (bpy) in combination with the compound $[Co_2(L^1SSL^1)(X)_4]$ (X = Cl, Br).[11] Unexpectedly, the reaction with bpy turned out to be rather cumbersome, and the ligand-field strength of bpy appeared to be not as large as was anticipated.[11] In the current study we employed a similar strategy, but now using the bidentate ligand 8−quinolinolate. In addition to having a strong ligand-field this ligand is anionic in nature, which might help stabilizing the charge of the Co(III) thiolate fragment.

Indeed, our experimental results show that the addition of $quin^-$ to both cobalt(II)-disulfide compounds [**1**$_{SS}$] and [**2**$_{SS}$] affords their respective cobalt(III)-thiolate compounds [**1**$_S$]Cl and [**2**$_S$]Cl in a clean manner, in contrast to the reactions with bpy. The unexpected formation of single crystals of [**2**$_{SSquin}$] provides valuable information about the reactivity of this compound. The crystal structure of [**2**$_{SSquin}$] shows that the L^2S fragment binds with the three

nitrogen donor atoms in meridional fashion, whereas in $[Co_2(L^1SSL^1)(bpy)_2(Cl_2)](BPh_4)_2$ the nitrogen donor atoms are in a facial arrangement.[11] In Chapter 2, we showed that formation of the cobalt(III)-thiolate compound with bpy is hampered by the fact that several donor atoms of the chelating ligands in this 'intermediate' compound have to dissociate and rearrange before redox-conversion can take place. In addition, DFT calculations showed that the highest singly occupied molecular orbital (SOMO) level of the meridional isomer of the 'intermediate' bpy compound is more destabilized than that of facial isomer; thus it is more difficult for electron transfer to occur in the observed 'intermediate' with facial arrangement of the nitrogen donor atoms.[11] The meridional orientation of the L^2SSL^2 ligand combined with the position of $quin^-$ in the structure of $[\mathbf{2}_{\mathbf{SSquin}}]$ provides space for the disulfide sulfur atom to approach the cobalt(II) center for electron transfer after dissociation of the chloride ions, to ultimately form the cobalt(III)-thiolate species $[\mathbf{2}_{\mathbf{S}}]^+$. Thus, the meridional orientation of the ligand L^2SSL^2 (and L^1SSL^1) might be the reason for the more facile conversion of the Co(II)-disulfide to the Co(III)-thiolate compounds when using $quin^-$ as the auxiliary ligand.

Using DFT studies, we revealed that the orientation of the asymmetric ligand $quin^-$ has a large effect on the stability of the thiolate compounds, as the experimentally obtained $[\mathbf{1}_{\mathbf{S}}]^+$ is 6 kcal/mol more stable than hypothetical $[\mathbf{1}_{\mathbf{S,rev}}]^+$ in methanol. This difference in stability is also observed for $[\mathbf{2}_{\mathbf{S}}]^+$, which is 5 kcal/mol more stable than $[\mathbf{2}_{\mathbf{S,rev}}]^+$. Activation-strain and energy-decomposition analyses show that the higher stability of $[\mathbf{1}_{\mathbf{S}}]^+$ is caused by more favorable electrostatic interactions between the fragments $[Co(L^1S)]^{2+}$ and $[quin]^-$ in $[\mathbf{1}_{\mathbf{S}}]^+$ compared to $[\mathbf{1}_{\mathbf{S,rev}}]^+$. The positively charged $[Co(L^1S)]^{2+}$ fragment and the negatively charged $[quin]^-$ fragment are closer in $[\mathbf{1}_{\mathbf{S}}]^+$ than in $[\mathbf{1}_{\mathbf{S,rev}}]^+$, causing stronger electrostatic interactions in $[\mathbf{1}_{\mathbf{S}}]^+$.

The ligand L^1SSL^1 has been studied extensively for potential redox-conversion reactions using copper(I), cobalt(II), and iron(II) salts, which were successful for copper and cobalt, but not for iron.[4, 8-10, 12, 28] It has been reported that the methylated ligand L^2SSL^2 in combination with a copper(I) salt in dichloromethane results in the formation of the corresponding Cu(II) thiolate complex,[9] whereas so far we were unsuccessful to trigger redox-conversion with cobalt(II) salts.[10] The introduction of two methyl groups in the ligand L^2SSL^2 has been shown to result in longer Co–N distances,[9, 10, 12] indicating a decrease of the donor ability of the pyridine nitrogen atom, resulting in lower ligand-field strength, thus

decreasing the chances of redox-conversion of its cobalt(II)-disulfide compound to the corresponding cobalt(III)-thiolate complex.[10] The red-shifts of about 10 nm in the UV-visible spectra of [**2**$_{SS}$] or [**2**$_{S}$]Cl compared to [**1**$_{SS}$] or [**1**$_{S}$]Cl, respectively, indicate that indeed the ligand L^2SSL^2 has a lower ligand-field strength than L^1SSL^1. Our DFT studies further confirm our experimental observations: the smaller energy difference of the highest and lowest MO in the set of orbitals with large cobalt *d*-orbital contribution of [**2**$_{S}$]$^+$ compared to that of [**1**$_{S}$]$^+$ is in agreement with the ligand-field strength of L^2SSL^2 being smaller than that of L^1SSL^1. Nevertheless, we now have shown that the conversion of the cobalt(II)-disulfide complex of L^2SSL^2 into cobalt(III)-thiolate compound [**2**$_{S}$]Cl can be achieved using an external ligand with large ligand-field strength, compensating for the lower ligand-field strength of L^2SSL^2.

3.4. Conclusion

The cobalt(III)-thiolate complexes [**1**$_{S}$]Cl and [**2**$_{S}$]Cl can be formed from a reaction of cobalt(II)-disulfide compound [**1**$_{SS}$] and [**2**$_{SS}$] in with the anionic bidentate ligand 8-quinolinolate. Clean conversion was achieved of the disulfide compounds to their respective thiolate compounds in high yields. Our experimental results in combination with DFT calculations show that despite the lower ligand-field strength of the ligand L^2SSL^2, conversion of the cobalt(II)-disulfide complex of L^2SSL^2 to the corresponding cobalt(III)-thiolate complex can be achieved with a strong-field ligand such as 8-quinolinolate. It appeared that the orientation of the asymmetric quin$^-$ ligand in the thiolate complexes is critical to their stability. The Co(III)-thiolate complexes benefits from more stabilizing electrostatic interactions when the oxygen donor of quin$^-$ is located *trans* to the thiolate donor. Overall, this study suggests that the redox-conversion of Co(II)-disulfide compounds to Co(III)-thiolate complexes is affected largely by the ligand-field strength of both the disulfide ligand and the additional ligand. However, important parameters to be considered also comprise the charge of the added ligand and the electronic effects caused by its orientation of the auxiliary ligand. Further research will be directed to assess the magnitude of these effects using various ligand systems, and to further expand the investigations with different transition metal ions.

3.5. Experimental Section

3.5.1. General

All reagents were purchased from commercial sources and were used as received unless noted otherwise. Degassed solvents used were obtained using the freeze-pump-thaw method followed by drying the solvents using the appropriate size of activated molecular sieves. The ligands L^1SSL^1, L^2SSL^2, and the cobalt compound $[Co_2(L^1SSL^1)Cl_4]$ [**1**$_{SS}$] were prepared according to previously published procedures.[8, 12] The ligand L^2SSL^2 was purified similarly to the ligand L^1SSL^1, by refluxing in petroleum ether followed by cooling instead of using column chromatography as reported. The synthesis of the cobalt compounds was performed using standard Schlenk-line techniques under an argon atmosphere. ^{1}H NMR spectra were recorded on a Bruker 300 DPX spectrometer at room temperature. Mass spectra were recorded on a Thermo Scientific MSQ Plus and Shimadzu LCMS 2020 mass spectrometer with electrospray ionization (ESI) method. Formic acid was added to the eluting solvent with the final concentration of 1% (v/v). Simulated mass spectra were generated using mMass (version 5.5.0) software.[29] IR spectra were obtained using a PerkinElmer Spectrum Two System equipped with Universal ATR module containing diamond crystal for single reflection (scan range 400-4000 cm^{-1}, resolution 4 cm^{-1}). Magnetic susceptibility measurements were performed on a Sherwood Scientific Magnetic Susceptibility Balance MK1, and the magnetic moments were calculated according to the literature.[30] Bond distances and angles analysis of the crystal structures were performed using the Mogul module on Mercury (version 4.3.1) software.[31] UV-visible spectra were collected using a transmission dip probe with variable path lengths and a reflection probe on an Avantes AvaSpec-2048 spectrometer and using an Avalight-DH-S-Bal light source. Elemental analyses were performed by the Microanalytical Laboratory Kolbe in Germany.

3.5.2. Single crystal X-ray crystallography

All reflection intensities were measured at 110(2) K using a SuperNova diffractometer (equipped with Atlas detector) with Mo *K*α radiation (λ = 0.71073 Å) under the program CrysAlisPro (Version CrysAlisPro 1.171.39.29c, Rigaku OD, 2017). The same program was used to refine the cell dimensions and for data reduction. The structure was solved with the program SHELXS-2018/3 and was refined on F^2 with SHELXL-2018/3.[32] Numerical absorption correction based on Gaussian integration over a multifaceted crystal model was

applied using CrysAlisPro. The temperature of the data collection was controlled using the system Cryojet (manufactured by Oxford Instruments). The H atoms were placed at calculated positions using the instructions AFIX 23, AFIX 43 or AFIX 137 with isotropic displacement parameters having values 1.2 or 1.5 U_{eq} of the attached C atoms. The structure of compound [**1**$_{\mathbf{S}}$]Cl is ordered. The structure of [**2**$_{\mathbf{SSquin}}$] is partly disordered. The asymmetric unit also contains one partially occupied ordered lattice MeCN solvent molecule (occupancy factor: 0.903(7)) and some amount of significantly disordered lattice molecules (MeCN). The structure of [**2**$_{\mathbf{S}}$**-Ag-2**$_{\mathbf{S}}$]$(SbF_6)_3$ is significantly disordered (the Cobalt complex and three SbF_6^- counterions are mostly disordered). The asymmetric unit also contains one ordered lattice acetonitrile solvent molecule, and some amount of very disordered (and possibly partially occupied) lattice solvent molecules. The contributions of the disordered moiety were removed from the final refinement using the SQUEEZE procedure in Platon.[33, 34]

3.5.3. Computational methods

All calculations were performed with the Amsterdam Density Functional (ADF) program version 2017.103 using Zeroth Order Regular Approximation (ZORA) scalar relativistic effect at OPBE functional and TZP basis set for geometry optimizations and energies.[35-38] Solvation of the molecule was simulated using the conductor-like screening model (COSMO) in methanol.[39] The stationary points were checked to be minima at potential energy surface using vibrational analysis. All the compounds were calculated with S=0, in agreement with our previous study. Time-Dependent Density Functional Theory (TDDFT) calculations for the simulation of the UV-visible spectra were done using Davidson's procedure with ZORA scalar relativistic effect and conductor-like screening model (COSMO) in acetonitrile.[40] The calculations were done for the lowest 10 excitations of the Co(III)-thiolate compounds and lowest 30 excitations of the Co(II)-disulfide compounds. The simulated spectra have been adjusted for clearer comparison with the experimental data, the spectra were red-shifted for [**1**$_{\mathbf{SS}}$] (22 nm) and [**2**$_{\mathbf{SS}}$] (20 nm) and blue-shifted for [**1**$_{\mathbf{S}}$]$^+$ (66 nm) and [**2**$_{\mathbf{S}}$]$^+$ (60 nm). Kohn-Sham molecular orbital (KS-MO) analysis for the determination of *d*-orbital splitting energies of the complex was done according to the published procedure on the optimized geometries of [**1**$_{\mathbf{S}}$]$^+$ and [**2**$_{\mathbf{S}}$]$^+$ in the gas phase.[11]

The bond energy (ΔE_{bond}) is given by Equation 3.1 and can be decomposed into the strain energy (ΔE_{strain}) and interaction energy (ΔE_{int}) (Equation 3.2). The strain energy is the energy needed to deform the fragments from their equilibrium geometries to their actual geometry in the complex. The interaction energy corresponds to the energy change when the deformed fragments are interacting with each other in the complex and can be further decomposed into electrostatic interaction energy (ΔV_{elstat}), Pauli repulsion energy (ΔE_{Pauli}), and orbital interaction energy (ΔE_{oi}) using energy-decomposition analysis (EDA, Equation 3.3). ΔV_{elstat} represents the Coulomb interaction between the unperturbed charge distributions of the two deformed fragments, which is usually an attractive interaction. ΔE_{Pauli} comprises of the destabilization energy associated with the interaction between occupied orbitals which is responsible for steric repulsion. The stabilizing ΔE_{oi} accounts for the charge-transfer, donor-acceptor interactions, and polarization.

$$\Delta E_{bond} = E_{optimized\ complex} - E_{optimized\ [Co(L^1S)]^{2+}} - E_{optimized\ [quin]^-} \quad \text{Equation 3.1.}$$

$$\Delta E_{bond} = \Delta E_{strain} + \Delta E_{int} \quad \text{Equation 3.2.}$$

$$\Delta E_{int} = \Delta V_{elstat} + \Delta E_{Pauli} + \Delta E_{oi} \quad \text{Equation 3.3.}$$

3.5.4. Synthesis of the compounds

[$Co_2(L^2SSL^2)(Cl)_4$] ([2ss])

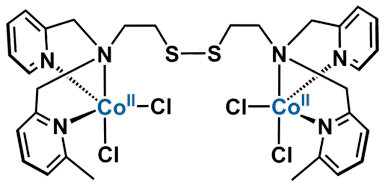

[$Co_2(L^2SSL^2)(Cl)_4$]

The compound was prepared similarly to compound [**1ss**],[8] using ligand L^2SSL^2 instead of L^1SSL^1. An intense purple powder was obtained in 72% yield. IR (neat, cm^{-1}): 3066w, 2924w, 1668w, 1605s, 1574m, 1442s, 1381m, 1364m, 1298w, 1225w, 1159m, 1090m, 1053m, 1017s, 960m, 860m, 765vs, 730m, 646m, 562w, 536w, 521w, 500w, 417m. UV−Visible spectra in acetonitrile: 545 nm ($\varepsilon = 1.5 \times 10^3\ M^{-1}\ cm^{-1}$), 652 nm ($\varepsilon = 8.5 \times 10^2\ M^{-1}\ cm^{-1}$), 850−950 nm ($\varepsilon < 100\ M^{-1}\ cm^{-1}$). ESI-MS found (calcd.) for [**2ss** – $4Cl^-$ + $2HCOO^-$]$^{2+}$ *m/z* 376.2 (376.04) and for [**2ss** – $2Cl^-$ + $HCOO^-$]$^+$ *m/z* 777.1 (777.05). Elemental analysis (%) for compound [**2ss**] ($C_{30}H_{36}Cl_4Co_2N_6S_2$), calcd. C, 44.79; H, 4.51; N, 10.45; found C, 44.72; H, 4.49; N, 10.43.

[Co(L[1]S)(8-quinolinolate)]Cl ([1s]Cl)

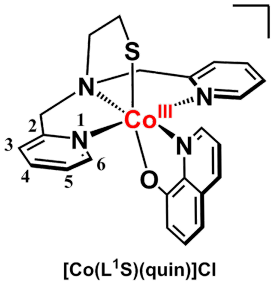

[Co(L[1]S)(quin)]Cl

The ligand L^1SSL^1 (52.35 mg, 0.101 mmol) was dissolved in 4 mL dry and deoxygenated methanol. Into the solution of the ligand, anhydrous $CoCl_2$ (26.25 mg, 0.202 mmol, 2 equiv. to the L^1SSL^1) was added. The resulting purple solution was stirred for 1 hour. In a separate flask under argon, 8-quinolinol (45.12 mg, 0.311 mmol) was added along with 44 µL of triethylamine (0.316 mmol, 1 equiv. to 8-quinolinol). Dry and deoxygenated methanol (1 mL) was added to dissolve the 8-quinolinol and triethylamine. From this solution, 680 µL (=0.202 mmol of 8-quinolinol, 2 equiv. to L^1SSL^1) was transferred to the purple solution of $[Co_2(L^1SSL^1)Cl_4]$. The color of the solution quickly changed into brown and the solution was stirred for 2 hours. The solution was further concentrated until approximately 1 mL was left in the flask. Into the flask, 10 mL dry and deoxygenated diethyl ether was added, resulting in the formation of a brown precipitate. The precipitate was then washed twice with 10 mL dry and deoxygenated diethyl ether, filtered, and then dried in vacuo. Yield: 96 mg, 0.193 mmol, 96%. Dark brown single crystals of compound [**1s**]Cl were grown after 2 days using vapor diffusion of dry and deoxygenated diethyl ether into a solution of [**1s**]Cl in a 1:1 mixture of dry and deoxygenated acetonitrile and methanol. IR (neat, cm^{-1}): 2945w, 2602m, 2496m, 1608w, 1570m, 1497s, 1461s, 1444m, 1397m, 1376s, 1321s, 1284m, 1223w, 1172m, 1111m, 1036m, 905w, 851w, 819m, 775m, 748s, 719w, 626m, 516s, 462m, 448m, 424m. ESI-MS calcd. for $[\mathbf{1s}]^+$ *m/z* 461.08, found *m/z* 461.1. ^{1}H-NMR (300 MHz, CD3CN, RT) δ(ppm): 1.29−1.33 (t, triethylamine.HCl), 1.84−1.87 (t, 2 H, N-CH_2-C**H**$_2$-S), 3.01−3.08 (q, triethylamine.HCl), 3.34−3.38 (t, 2H, N-C**H**$_2$-CH_2-S), 4.57−4.62 and 5.45−5.50 (d, 4H, py-C**H**$_2$-N), 6.87−6.90 (dd, 1H, ortho−C**H**-O(quin$^-$)), 7.06−7.09 (dd, 1H, para−C**H**-O(quin$^-$)), 7.13−7.17 (t, 2H, 2**H**$_4$(py)), 7.25−7.27 (dd, 2H, 2**H**$_3$(py)), 7.37−7.42 (t, 1H, meta−C**H**-O(quin$^-$)), 7.46−7.48 (d, 2H, 2**H**$_6$(py)), 7.85−7.88 (3H, m, meta−C**H**-N(quin$^-$) and 2**H**$_5$(py)), 8.50−8.53 (dd, 1H, para−C**H**-N(quin$^-$)), 9.04−9.06 (dd, 1H, ortho−C**H**-N(quin$^-$)). Elemental analysis (%) for compound [**1s**]Cl·1.5 H_2O ($C_{23}H_{22}ClCoN_4OS$·1.5 H_2O), calcd. C, 52.73; H, 4.81; N, 10.69; found C, 52.86; H, 4.67; N, 10.58.

[Co(L²S)(8-quinolinolate)]Cl ([2s]Cl)

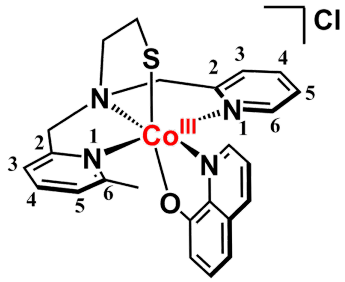

[Co(L²S)(quin)]Cl

Compound [**2s**]Cl was obtained using a similar procedure as for compound [**1s**]Cl but using L^2SSL^2 instead of L^1SSL^1. Yield: 102 mg, 0.2 mmol, 99%. Dark brown single crystals of compound [**2s-Ag-2s**]$(SbF_6)_3$ were grown after two days using vapor diffusion of diethyl ether into an acetonitrile solution containing [**2s**]Cl and one equivalent of $AgSbF_6$. IR (neat, cm^{-1}): 3391br, 2978w, 2603w, 2497w, 1608w, 1568m, 1497s, 1462s, 1447m, 1381s, 1322s, 1289w, 1225w, 1173w, 1111m, 1067w, 1037m, 960w, 902w, 830m, 807m, 776m, 748s, 726w, 650m, 624m, 517s, 462w, 436w, 413w. ESI-MS calcd. for $[\mathbf{2s}]^+$ *m/z* 475.1, found *m/z* 475.3. ^{1}H-NMR (300 MHz, CD_3CN, RT): 1.26−1.31 (t, triethylamine.HCl), 1.78 (s, 3H, py-C**H₃**), 2.98−3.05 (q, triethylamine.HCl), 3.18−3.50 (m, 2H, N-C**H₂**-CH_2-S and N-CH_2-C**H₂**-S, the other two protons overlaps with the solvent peaks at around 1.9 ppm), 4.50−4.62, 5.43−5.48, and 5.75−5.80 (d, d, t, 4H, N-C**H₂**-py and N-C**H₂**-pyMe), 6.89−6.92 (d, 1H, ortho−C**H**-O(quin⁻)), 6.92−6.95 (dd, 1H, **H₅**(pyMe)), 7.01−7.07 (td, 2H, 2**H₃**(py and pyMe)), 7.08−7.12 (t, 1H, para−C**H**-N(quin⁻)), 7.27−7.29 (d, 1H, para−C**H**-O(quin⁻)), 7.36−7.41 (t, 2H, meta−C**H**-N(quin⁻) and meta−C**H**-O(quin⁻)), 7.66−7.72 (t, 1H, **H₅**(py)), 7.75−7.82 (m, 2H, 2**H₄**(py and pyMe)), 8.47−8.50 (dd, 1H, **H₆**(py)), 9.26−9.29 (dd, 1H, ortho−C**H**-N(quin⁻)). Elemental analysis (%) for compound [**2s**]Cl· H_2O ($C_{24}H_{25}ClCoN_4OS \cdot H_2O$), calcd. C, 54.50; H, 4.95; N, 10.59; found C, 54.26; H, 4.79; N, 10.49.

3.6. References

1. Martin, D. R. and Matyushov, D. V. *Sci. Rep.* **2017**, 7, 1-11.
2. Li, Y., Park, J.-S., Deng, J.-H. and Bai, Y. *J. Bioenerg. Biomembr.* **2006**, 38 (5-6), 283-291.
3. Riebe, O., Fischer, R. J., Wampler, D. A., Kurtz, D. M. and Bahl, H. *Microbiology (Reading)* **2009**, 155 (Pt 1), 16-24.
4. Ueno, Y., Tachi, Y. and Itoh, S. *J. Am. Chem. Soc.* **2002**, 124 (42), 12428-12429.
5. Gennari, M., Brazzolotto, D., Yu, S., Pecaut, J., Philouze, C., Rouzieres, M., Clerac, R., Orio, M. and Duboc, C. *Chem. Eur. J.* **2015**, 21 (51), 18770-18778.
6. Gennari, M., Gerey, B., Hall, N., Pecaut, J., Collomb, M.-N., Rouzieres, M., Clerac, R., Orio, M. and Duboc, C. *Angew. Chem. Int. Ed.* **2014**, 53 (21), 5318-5321.
7. Wang, L., Reinhard, F. G. C., Philouze, C., Demeshko, S., de Visser, S. P., Meyer, F., Gennari, M. and Duboc, C. *Chem. Eur. J.* **2018**, 24 (46), 11973-11982.
8. Jiang, F., Siegler, M. A., Sun, X., Jiang, L., Fonseca Guerra, C. and Bouwman, E. *Inorg. Chem.* **2018**, 57 (15), 8796-8805.

9. Ording-Wenker, E. C. M., van der Plas, M., Siegler, M. A., Bonnet, S., Bickelhaupt, F. M., Fonseca Guerra, C. and Bouwman, E. *Inorg. Chem.* **2014**, 53 (16), 8494-8504.
10. Jiang, F., Marvelous, C., Verschuur, A. C., Siegler, M. A., Teat, S. J. and Bouwman, E. *Inorg. Chim. Acta* **2022**, 120880.
11. Marvelous, C., de Azevedo Santos, L., Siegler, M. A., Fonseca Guerra, C. and Bouwman, E. *Dalton Trans.* **2022**, 51, 8046-8055.
12. Itoh, S., Nagagawa, M. and Fukuzumi, S. *J. Am. Chem. Soc.* **2001**, 123 (17), 4087-4088.
13. Franz, K. J., Doerrer, L. H., Spingler, B. and Lippard, S. J. *Inorg. Chem.* **2001**, 40 (15), 3774-3780.
14. Dey, S., Todorova, T. K., Fontecave, M. and Mougel, V. *Angew. Chem. Int. Ed.* **2020**, 59 (36), 15726-15733.
15. Lonnon, D. G., Craig, D. C. and Colbran, S. B. *Inorg. Chem. Commun.* **2003**, 6 (11), 1351-1353.
16. Zhu, C.-Y., Zhang, Y.-Q., Liao, R.-Z., Xia, W., Hu, J.-C., Wu, J., Liu, H. and Wang, F. *Dalton Trans.* **2018**, 47 (37), 13142-13150.
17. Janiak, C. *J. Chem. Soc., Dalton Trans.* **2000**, (21), 3885-3896.
18. Konno, T., Kawamoto, T., Kuwabara, R., Yoshimura, T. and Hirotsu, M. *Chem. Lett.* **2002**, (3), 304-305.
19. Tamura, M., Yoshinari, N., Igashira-Kamiyama, A. and Konno, T. *Acta Crystallogr. Sect. Sect. E: Struct. Rep. Online* **2007**, 63, M1641-U629.
20. Yoshinari, N., Chikamoto, Y., Iwata, M., Kawamoto, T. and Konno, T. *Bull. Chem. Soc. Jpn.* **2006**, 79 (7), 1066-1068.
21. Yoshinari, N., Igashira-Kamiyama, A. and Konno, T. *Acta Crystallogr. Sect. Sect. E: Struct. Rep. Online* **2006**, 62, M1229-M1231.
22. Chan, S. L.-F., Lam, T. L., Yang, C., Lai, J., Cao, B., Zhou, Z. and Zhu, Q. *Polyhedron* **2017**, 125, 156-163.
23. Massoud, S. S., Broussard, K. T., Mautner, F. A., Vicente, R., Saha, M. K. and Bernal, I. *Inorg. Chim. Acta* **2008**, 361 (1), 123-131.
24. Pal, A. K., Li, C., Hanan, G. S. and Zysman-Colman, E. *Angew. Chem. Int. Ed.* **2018**, 57 (27), 8027-8031.
25. Bickelhaupt, F. M. and Houk, K. N. *Angew. Chem. Int. Ed.* **2017**, 56 (34), 10070-10086.
26. Vermeeren, P., Van Der Lubbe, S. C. C., Fonseca Guerra, C., Bickelhaupt, F. M. and Hamlin, T. A. *Nature Protocols* **2020**, 15 (2), 649-667.
27. Bickelhaupt, F. M. and Baerends, E. J., *Reviews in Computational Chemistry*: *Reviews in Computational Chemistry, Vol 15*, **2000**, Vol. 15, 1-86.
28. Jiang, F., Siegler, M. A. and Bouwman, E. *Inorg. Chem. Commun.* **2018**, 94, 53-56.
29. Strohalm, M., mMass - Open Source Mass Spectrometry Tool. www.mmass.org
30. Bain, G. A. and Berry, J. F. *J. Chem. Educ.* **2008**, 85 (4), 532-536.
31. Macrae, C. F., Sovago, I., Cottrell, S. J., Galek, P. T. A., McCabe, P., Pidcock, E., Platings, M., Shields, G. P., Stevens, J. S., Towler, M. and Wood, P. A. *J. Appl. Crystallogr.* **2020**, 53, 226-235.
32. Sheldrick, G. M. *Acta Crystallogr. Sect. A: Found. Crystallogr.* **2008**, 64, 112-122.
33. Spek, A. L. *Acta Crystallogr. Sect. C: Cryst. Struct. Commun.* **2015**, 71 (Pt 1), 9-18.
34. Spek, A. L. *Acta Crystallogr. Sect. D. Biol. Crystallogr.* **2009**, 65 (2), 148-155.
35. ADF2017.107. SCM Theoretical Chemistry, Vrije Universiteit: Amsterdam, The Netherlands, www.scm.com
36. Swart, M., Ehlers, A. W. and Lammertsma, K. *Mol. Phys.* **2004**, 102 (23-24), 2467-2474.
37. Van Lenthe, E. and Baerends, E. J. *J. Comput. Chem.* **2003**, 24 (9), 1142-1156.
38. Van Lenthe, E., Baerends, E. J. and Snijders, J. G. *J. Chem. Phys.* **1994**, 101 (11), 9783-9792.
39. Klamt, A. and Schuurmann, G. *J. Chem. Soc., Perkin Trans. 2* **1993**, (5), 799-805.
40. Rosa, A., Baerends, E. J., van Gisbergen, S. J. A., van Lenthe, E., Groeneveld, J. A. and Snijders, J. G. *J. Am. Chem. Soc.* **1999**, 121 (44), 10356-10365.